Evolution of the charge density wave superstructure in $ZrTe_3$ under pressure

Moritz Hoesch,[1] Gaston Garbarino,[2] Corsin Battaglia,[3] Philipp Aebi,[4] and Helmuth Berger[5]
[1]*Diamond Light Source, Harwell Campus, Didcot OX11 0DE, United Kingdom*
[2]*European Synchrotron Radiation Facility, 6 rue Jules Horowitz, 38043 Grenoble Cedex, France*
[3]*Empa, Swiss Federal Laboratories for Materials Science and Technology, Laboratory Materials for Energy Conversion, 8600 Dübendorf, Switzerland*
[4]*Département de Physique and Fribourg Center for Nanomaterials, Université de Fribourg, 1700 Fribourg, Switzerland*
[5]*Ecole Polytechnique Federale de Lausanne, Institut de physique de la matière complexe, 1015 Lausanne, Switzerland*
(Received 25 September 2015; revised manuscript received 18 January 2016; published 1 March 2016)

The material $ZrTe_3$ is a well-known example of an incommensurate periodic lattice distortion (PLD) at low temperatures due to a charge density wave (CDW). Previous studies have found a sharp boundary as a function of pressure between CDW below 5 GPa and bulk superconductivity above this value. We present a study of low-temperature-high-pressure single crystal x-ray diffraction along with *ab initio* density functional theory calculations. The modulation vector q_{CDW} is found to change smoothly with pressure until the PLD is lost. Fermi surface calculations reproduce these changes, but neither these nor the experimental crystal lattice structure show a particular step change at 5 GPa, thus leading to the conclusion that the CDW is lost accidentally by tipping the balance of CDW formation in the Fermi surface nesting that stabilizes it.

DOI: 10.1103/PhysRevB.93.125102

The quest to understand the competition between the charge density wave (CDW) modulation and superconductivity (SC) as two possible ground states of metals has recently been refueled by the discovery of competition between the nonconventional high temperature superconductivity of $YBa_2Cu_3O_{6+x}$ (YBCO) and a periodically modulated lattice distortion [1,2] that is also coupled to a strong phonon anomaly [3]. The CDW is a generally incommensurate electronic ordering phenomenon, accompanied and usually experimentally detected by a periodic lattice distortion (PLD) [4]. In the Peierls picture it is thought to be driven by Fermi surface (FS) nesting, and the energy gain due to modulation is derived from removal of density of states from the Fermi energy E_F (CDW gap). Superconductivity is also derived from momentum space correlations of the motion of the electrons (k-space pairing). The competition between the two can arise from the need for a finite density of states at E_F for superconductivity to occur. In a multiband system a coexistence is also possible if the driving electrons for SC and CDW are in different sheets of the FS. In the transition metal chalogenide class of materials we investigate here the superconductivity is assumed to be of conventional electron-phonon coupling driven character and has its highest transition temperature at $T_c = 7.2$ K in 2H-$NbSe_2$ [5].

In this paper we present a study of the crystal lattice of $ZrTe_3$ under hydrostatic pressure with a focus on the PLD at temperatures below the CDW transition temperature T_{CDW}. We do not probe the superconducting state itself. The phase boundaries of the CDW state observed in our experiment are, however, fully consistent with the observation of a previous study [6], and thus we infer that the sample would show the same bulk superconductivity when the critical pressure is exceeded (5 GPa) and below the superconducting transition temperature $T_c \simeq 4$ K.

$ZrTe_3$ has a crystal structure with building blocks related to the prototypical $NbSe_3$ [7] but with the CDW modulation in the nearly equidistant chains of Te atoms Te(2)-Te(3) along the a lattice direction below the transition temperature $T_{CDW} = 63$ K [8] and modulation $q_{CDW} = (0.07\ 0\ 0.3333)$ [9]. The phase transition is a soft-phonon transition with signatures of the low-dimensional nature [10]. Nesting of a quasi-one-dimensional ("q1D") Fermi surface sheet derived from Te p_σ states oriented along a on the Te chains was identified to be the driving mechanism of the CDW [11,12]. This theoretical assignment is supported by the observation of a gap in the electronic structure by angle-resolved photoelectron spectroscopy [13]. $ZrTe_3$ thus shows all three experimental signatures of a CDW (resistivity anomaly, PLD, and gap in the electronic structure), yet a quantitative consistency of calculated nesting and observed PLD modulation was never achieved and the formation of the CDW may be more complicate than the Peierls picture suggest. For a full review of experimental findings on CDWs the reader is referred to Ref. [14].

Filamentary superconductivity with a broad transition around 2 K is observed at ambient pressure [15,16]. This is lost completely under hydrostatic pressure while T_{CDW} rises to about 100 K around 2 GPa and decreases again. At 5 GPa the CDW signature is suddenly lost and a sharp superconducting transition with $T_c \approx 2$ K is observed in electrical transport experiments [6]. In the pressure range up to 4 GPa the effects of the charge density wave formation of the crystal lattice have been investigated by vibrational Raman spectroscopy [17]. At ambient pressure, bulk superconductivity can also be found in $ZrTe_3$ crystals with Ni [18] or Cu [19] intercalations or with disorder [20]. These studies thus point at the importance of disorder for the emergence of as superconducting state. Our present study, as well as the study in Ref. [6] on the other hand, assumes ordered material, and we have no evidence of any disorder or reduction in crystal quality at pressures exceeding 5 GPa.

The schematic view of the FS of $ZrTe_3$ is shown in Fig. 1 along an *ab initio* calculation at ambient pressure. The central rounded "2D" Fermi surface sheet and the flatter "q1D" sheets are marked. The latter are really two sheets due to the two inequivalent Te atoms in the chains. They are very flat in a large region around the D and E points and more warped and

 ©2016 American Physical Society

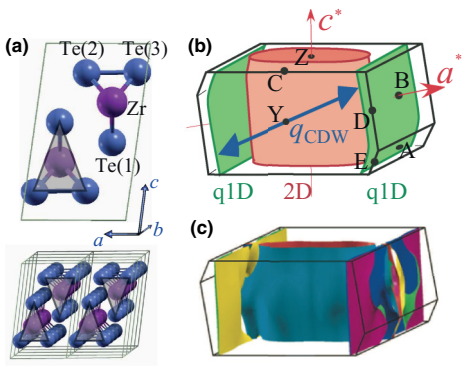

FIG. 1. (a) Crystal structure of $ZrTe_3$. (b) Schematic view of the two main sheets of the Fermi surface of $ZrTe_3$ ("2D" and "q1D") in the monoclinic first Brillouin zone with various high symmetry points marked. The CDW modulation vector (0.93 0 0.666) is marked by a blue arrow. (c) *Ab initio* calculated Fermi surface of $ZrTe_3$ at ambient pressure.

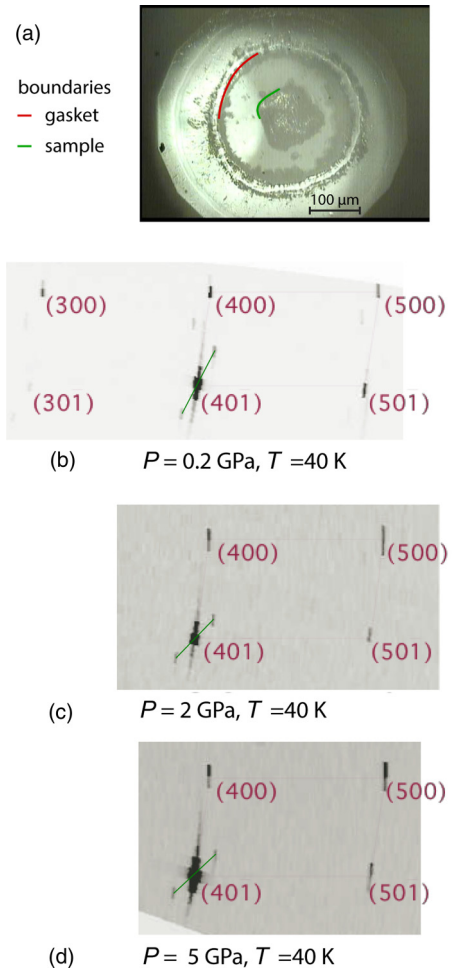

FIG. 2. (a) Micrograph of the sample inside the DAC before full pressurization. The bright area is the culot of the diamonds, and the contours of the gasket hole and the sample are marked with red and green lines, respectively. (b)–(d) Reconstructed diffraction patterns of $ZrTe_3$ in a diamond anvil cell at pressures $P = 0.2$, 2, 5 GPa. A part of the a^*–c^* plane is shown at $b^* = 0$. The reciprocal space modulation direction through the PLD superstructure spots adjacent to $(40\bar{1})$ is marked by a fine green line in each panel.

featuring complicated small pockets around B and A. The spanning vector shown is $[(1\ 0\ 1) - q_{CDW}]$ which serves to visualize the nesting across the Brillouin zone (BZ). A CDW gap in this sheet was observed by electron spectroscopy at low temperatures, while the "2D" sheet remains ungapped [13].

We have measured the x-ray diffraction pattern from a single crystal of $ZrTe_3$ at low temperatures ($T = 40$ K) and hydrostatic pressures up to 6 GPa generated by a membrane driven diamond anvil cell (DAC) using helium as the pressure transmitting medium. The pressure was measured using the fluorescence lines of a ruby chip placed close to the sample. The x-ray's wavelength was 0.3738 Å and the detector was a large area MAR CCD. The data were collected by a 1 degree step rotations of the sample in the x-ray beam, within the opening angle of the DAC. The platelet-shaped single crystal was located in the center of the gasket hole with the c axis close to the x-ray beam propagation direction. Reconstructed high symmetry planes of x-ray scattering intensities are shown in Fig. 2. The incommensurate PLD superstructure spots are readily observed close to the main lattice Bragg spot $(40\bar{1})$. These incommensurate superstructure spots remain sharp and clearly visible against the background up to pressures of 5 GPa (see Fig. 2) thus demonstrating that the single crystal remains intact and the crystal lattice well ordered up to these high pressures where the gasket hole [Fig. 2(b)] is significantly reduced in size and could thus squeeze the comparably soft crystal. No such squeezing was observed.

From the location of the superstructure spots relative to the main lattice spots we observe, strikingly, that the superstructure modulation vector q_{CDW} changes as a function of pressure, both in magnitude and angle. The modulation remains strictly in the (a^*, c^*)-plane ($q_b = 0$, not shown), but with increasing pressure it rotates away from the c^* axis towards a^*. The CDW modulation is analyzed in terms of the a^* and c^* components of q_{CDW} and the results are shown in Fig. 4. We observe that the a^* component gently increases in its value to a value of nearly 0.1 r.l.u (relative lattice units)

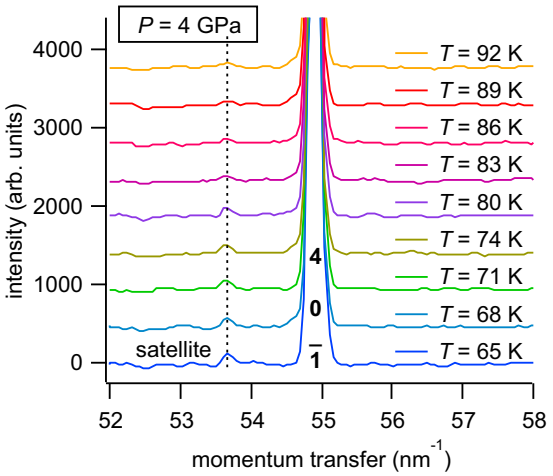

FIG. 3. Intensity profiles through the Bragg spot $(40\bar{1})$ along the PLD modulation direction as a function of temperature. On the left the satellite peak is observed up to temperatures of 90 K, above which none is observed, thus marking the phase boundary between the CDW state and the nonmodulated state.

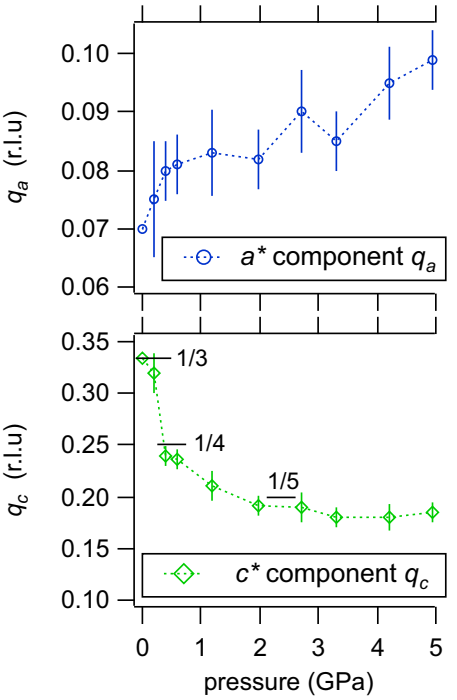

FIG. 4. Reciprocal lattice components of the CDW modulation vector q_{CDW} as a function of pressure. The a^* and c^* components are shown separately.

corresponding to a modulation wavelength of 10 unit cells along this direction. The c^* component first rapidly decreases to just below 0.25 r.l.u. and is then further reduced to a saturated value below 0.2 r.l.u.

We can now investigate the phase diagram of the CDW state. For the data at $T = 40$ K measurement temperature at pressures above 5 GPa no CDW superstructure is observed, as is also the case for room temperature data. At constant pressure below 5 GPa we can trace the CDW spots as a function of temperature as shown in Fig. 3 for the case of $P = 4$ GPa and the intensity disappears at a $T_{CDW} = 90$ K. Similar scans at ambient pressure give the well-known $T_{CDW} = 63$ K and at intermediate pressures the PLD also disappears at temperatures compatible with the phase diagram of the CDW deducted from transport measurements [6]. At constant pressure, the CDW modulation q_{CDW} remains constant through the observed temperature ranges (40 K - T_{CDW}).

Ab initio calculations of the electronic structure have been performed in two steps. First the atomic structure (lattice parameters and internal atomic positions) was relaxed under the constraint of the applied hydrostatic pressure in the program ABINIT [21] using density functional theory in local density approximation (LDA-DFT). These calculations have previously been reported [22]. With these atomic positions the all-electron band structure and Fermi surface was calculated by the full-potential method using generalized gradient approximation implemented in the Wien2k code, also including spin-orbit interaction energies [23]. The thus calculated Fermi surfaces are shown in Figs. 1(b) (ambient pressure) and 5 (various pressures up to 8 GPa).

The ambient pressure calculations are readily related to experiments of photoelectron spectroscopy [13,22,24] and the features of the Fermi surface are experimentally confirmed. At elevated pressure no such data can be obtained as the surface is embedded in the pressure medium and the photoelectrons cannot travel to the detector. The comparison at ambient pressure shows that small FS pockets around Γ and B seen

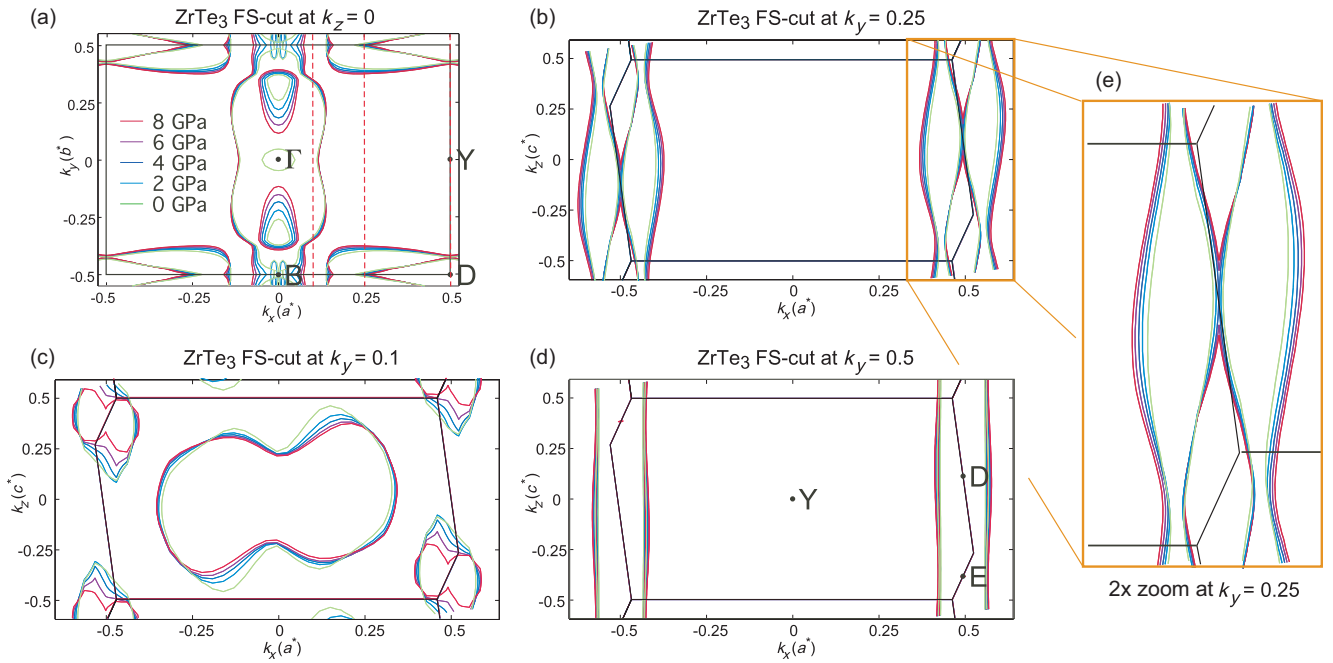

FIG. 5. *Ab- initio* calculated Fermi surface contours in various planes indicated by the axis labels and the offset in the title of each panel at five different pressures from ambient to well beyond the observation range of the CDW. Dashed lines in panel (a) indicate the cuts of panels (b), (c), and (d). Panel (e) on the right shows a 2× magnified view of panel (d) with the cut in the a^*–c^* plane ($k_x - k_y$) at $k_y = 0.25$ r.l.u.

in Figs. 5(a) and 5(b) are artifacts due to slightly imbalanced charges in the calculation. These bands are observed fully occupied in the experiment, thus not contributing to the FS, while the "2D" and "q1D" FS sheets have an excellent match between calculation and experiment [24]. The electronic structure along the BZ boundary, where the "q1D" FS sheet is found to match the experiment very well for a large region around the D and E points ($k_y \geqslant 0.2$ r.l.u.), where the gapped FS sheet is found. While the small artifact pockets evolve with increasing pressure [Figs. 5(a) and 5(b)], the "2D" sheet and in particular the "q1D" FS hardly change. Virtually no change is observed close to the line connecting D and E at $k_y = 0.5$ [Fig. 5(d)]. In the intermediate positions around $k_y = 0.25$ [Figs. 5(c) and 5(e)] we observe a systematic evolution. The Fermi wave vector of the outer FS sheet gradually moves away from the BZ boundary. Since this is a small electron pocket located around the BZ boundary this change corresponds to a slight increase in the occupation of the "q1D" band.

A test of any change of the crystal structure in the pressure range under investigation was performed in a separate x-ray diffraction experiment at room temperature using the same DAC set-up as the low temperature data. These data were analyzed with the Crysalis software [25]. Crysalis is optimized for indexing of single crystal diffraction patterns, thus the lattice parameters a, b, and c show rather large fluctuations and correlations. The cell volume V on the other hand is extracted reliably and has a much smaller error associated with it. It should be noted that due to the constrained geometry of the DAC we were not able to collect a sufficiently large set of diffraction spots to perform a full analysis of all atomic positions within the cell. The data are, however, consistent with a largely unchanged atomic arrangement and diffraction features, both at room temperature, as well as at low temperature remain sharp and well-defined (see Fig. 2). This is in contrast to the findings of Ref. [17], which reports a decrease of intensity of Raman signals that is associated with a structural degradation already from 1 GPa. We have no indication of any structural changes from our data, and the cell volume evolves smoothly and consistently across the whole pressure range. From the cell volume V as a function of pressure we can derive the compressibility as $\frac{1}{V}\frac{\partial V}{\partial P} = 1.6 \times 10^{-2}$ GPa^{-1}.

The calculations were thus also constrained to the $P21/m$ monoclinic symmetry throughout the pressure range. From Fig. 6 it is immediately visible that the lattice parameters and cell volume are systematically calculated to be 3.2% smaller than the measured parameters. The compressibility derived from the calculations is found to match the experimental value. A small contribution to the systematic discrepancy of lattice parameters between experiment and theory derives from thermal expansion, as the data were collected at room temperature, while the calculations correspond to the ground state. A much larger contribution arises from the bond shortening effect in LDA [26,27], which systematically underestimates lattice parameters. This effect can also be considered as an additional pressure term that shifts the effective pressure scale. Note that this effect is most pronounced along the b axis of the lattice, where covalent bonding is most prominent. For this reason the calculations were performed over a sufficiently large pressure range up to 8 GPa so that the relevant range around 5 GPa is certainly contained in the range.

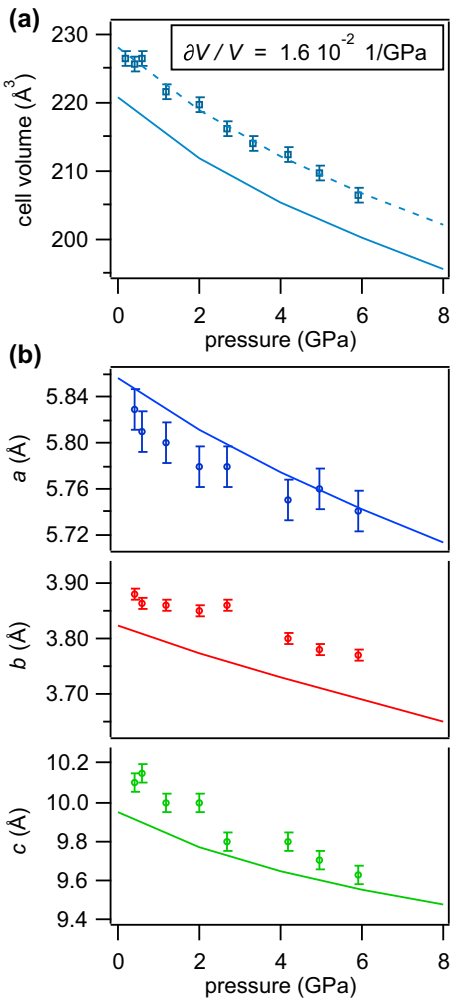

FIG. 6. Lattice parameters (b) and unit cell volume (a) as a function of pressure at room temperature and from calculations. The experimental data are shown as markers with error estimates and the calculated data as lines. In (a) the calculated data multiplied by 1.033 are reproduced as a dashed line to enable direct comparison despite the systematic discrepancy that is discussed in the text.

We are thus left with a puzzling nonobservation of any abrupt changes that could explain the loss of the CDW at 5 GPa. The lattice parameters (cell volume) evolve smoothly across this limit, the calculations match this and show a smooth evolution of increasing the band filling of the q1D band without changes in the topology and only minor changes in the topography of the Fermi surface, namely an increase in the nesting vector a^* component due to the increased band filling. Yet the PLD, which shows the extraordinary change of modulation vector as a function of pressure, is abruptly lost at the 5 GPa boundary. We thus have to conclude that the loss of the CDW state is caused by a shift of balance that stabilizes the CDW state at low pressures and which gets out of bounds, almost accidentally, at the 5 GPa pressure. From this basis we can now speculate about the emergence of proper superconductivity in the regime above 5 GPa, reported in Ref. [6], and we believe that this is due to having charge carriers at the Fermi energy available for the superconducting condensate, and these charge carriers have

a suitable electron-phonon coupling as manifest through the fact that at lower pressures the same band can stabilize the incommensurate Peierls distorted phase (CDW phase).

In summary we have investigated the CDW superstructure and found that the modulation vector q_{CDW} changes with pressure and disappears at the previously reported phase boundary of 5 GPa [6]. We rule out a change of the underlying crystal structure from data by the same x-ray diffraction method at room temperature. For ease of analysis, the evolution of q_{CDW} is separated into the a^* component, which gradually increases with pressure and the c^* component that decreases and then saturates. The evolution of the a^* component is supported by a slight increase in the band filling of the corresponding "q1D" FS sheet, thus leading to an increase of the nesting vector. The associated calculations support the experiment well, but the evolution of the Fermi surface shows no particular jump and thus the loss of the CDW state above 5 GPa can be considered as accidental. We speculate the superconductivity is enabled due to removal of its competitor, the CDW, and is supported by the same q1D band.

We wish to thank P. Monceau, P. Foury-Leylekian, and J.-P. Pouget for fruitful discussions over our data. A. Mirone's help with setting up calculations is acknowledged. K. Refson has kindly contributed to the discussion of overbonding. The experiment was performed at beamline ID27 at the European Synchrotron Radiation Facility (ESRF). Partial support for the experiments was provided by the Fonds National Suisse pour la Recherche Scientifique through Div. II.

[1] J. Chang, E. Blackburn, A. T. Holmes, N. B. Christensen, J. Larsen, J. Mesot, R. Liang, D. A. Bonn, W. N. Hardy, A. Watenphul *et al.*, Nat. Phys. **8**, 871 (2012).
[2] G. Ghiringhelli, M. Le Tacon, M. Minola, S. Blanco-Canosa, C. Mazzoli, N. B. Brookes, G. M. De Luca, A. Frano, D. G. Hawthorn, F. He *et al.*, Science **337**, 821 (2012).
[3] M. Le Tacon, A. Bosak, S. M. Souliou, G. Dellea, T. Loew, R. Heid, K.-P. Bohnen, G. Ghiringhelli, M. Krisch, and B. Keimer, Nat. Phys. **10**, 52 (2013).
[4] G. Grüner, *Density Waves in Solids*, Vol. 89 of *Frontiers in Physics* (Perseus publishing, Cambridge MA, 1994).
[5] I. Guillamón, H. Suderow, S. Vieira, L. Cario, P. Diener, and P. Rodière, Phys. Rev. Lett. **101**, 166407 (2008).
[6] R. Yomo, K. Yamaya, M. Abliz, M. Hedo, and Y. Uwatoko, Phys. Rev. B **71**, 132508 (2005).
[7] J. A. Wilson, Phys. Rev. B **19**, 6456 (1979).
[8] S. Takahashi, T. Sambongi, and S. Okada, J. Phys. (Paris), Colloq. **44**, C3 (1983).
[9] D. J. Eaglesham, J. W. Steeds, and J. A. Wilson, J. Phys. C **17**, L697 (1984).
[10] M. Hoesch, A. Bosak, D. Chernyshov, H. Berger, and M. Krisch, Phys. Rev. Lett. **102**, 086402 (2009).
[11] K. Stöwe and F. Wagner, J. Solid State Chem. **138**, 160 (1998).
[12] C. Felser, E. Finckh, H. Kleinke, and W. Tremel, J. Mater. Chem. **8**, 1787 (1998).
[13] T. Yokoya, T. Kiss, A. Chainani, S. Shin, and K. Yamaya, Phys. Rev. B **71**, 140504(R) (2005).
[14] P. Monceau, Adv. Phys. **61**, 325 (2012).
[15] H. Nakajima, K. Nomura, and S. Sambongi, Physica B **143**, 240 (1986).
[16] K. Yamaya, S. Takayanagi, and S. Tanda, Phys. Rev. B **85**, 184513 (2012).
[17] S. L. Gleason, Y. Gim, T. Byrum, A. Kogar, P. Abbamonte, E. Fradkin, G. J. MacDougall, D. J. Van Harlingen, X. Zhu, C. Petrovic *et al.*, Phys. Rev. B **91**, 155124 (2015).
[18] L. H, X. Zhu, and C. Petrovic, Europhys. Lett. **95**, 17011 (2011).
[19] X. Zhu, H. Lei, and C. Petrovic, Phys. Rev. Lett. **106**, 246404 (2011).
[20] X. Zhu, B. Lv, F. Wei, Y. Xue, B. Lorenz, L. Deng, Y. Sun, and C.-W. Chu, Phys. Rev. B **87**, 024508 (2013).
[21] X. Gonze, J.-M. Beuken, R. Caracas, F. Detraux, M. Fuchs, G.-M. Rignanese, L. Sindic, M. Verstaete, G. Zerah, F. Jollet *et al.*, Comput. Mater. Sci. **25**, 478 (2002).
[22] P. Starowicz, C. Battaglia, F. Clerc, L. Despont, A. Prodan, H. van Midden, U. Szerer, A. Szytula, M. Garnier, and P. Aebi, J. Alloys Compd. **442**, 268 (2007).
[23] P. Blaha, K. Schwarz, G. Madsen, D. Kvasnicka, and J. Luitz, *An Augmented Plane Wave Plus Local Orbitals Program for Calculating Crystal Properties* (Techn. Universität Wien, Austria, 2001).
[24] M. Hoesch, X. Cui, K. Shimada, C. Battaglia, S.-i. Fujimori, and H. Berger, Phys. Rev. B **80**, 075423 (2009).
[25] Crysalis ccd, crysalis red and associated programs (2006), oxford Diffraction Ltd Abingdon Oxfordshire England.
[26] R. O. Jones and O. Gunnarsson, Rev. Mod. Phys. **61**, 689 (1989).
[27] P. Haas, F. Tran, and P. Blaha, Phys. Rev. B **79**, 085104 (2009).